MECHANOCHEMISTRY

Acceleration of Diels-Alder reactions by mechanical distortion

Yerzhan S. Zholdassov^{1,2,3}, Li Yuan⁴, Sergio Romero Garcia⁵, Ryan W. Kwok^{2,3}, Alejandro Boscoboinik⁴, Daniel J. Valles^{1,2,3}, Mateusz Marianski^{2,3}, Ashlie Martini⁵, Robert W. Carpick⁴, Adam B. Braunschweig^{1,2,3}*

Challenges in quantifying how force affects bond formation have hindered the widespread adoption of mechanochemistry. We used parallel tip-based methods to determine reaction rates, activation energies, and activation volumes of force-accelerated [4+2] Diels-Alder cycloadditions between surface-immobilized anthracene and four dienophiles that differ in electronic and steric demand. The rate dependences on pressure were unexpectedly strong, and substantial differences were observed between the dienophiles. Multiscale modeling demonstrated that in proximity to a surface, mechanochemical trajectories ensued that were distinct from those observed solvothermally or under hydrostatic pressure. These results provide a framework for anticipating how experimental geometry, molecular confinement, and directed force contribute to mechanochemical kinetics.

he great majority of organic reactions carried out in industry and research laboratories rely on strictly solvothermal activation, in which solvent and heat act in concert to drive reactions along a trajectory toward products (1). The organic solvents used in these reactions account for >60% of all chemical manufacturing waste (2) and are often toxic (3), while as a result of the energy demand of solvothermal syntheses, the chemical industry consumes 37% of the total energy used in manufacturing (4). As such, there is a critical need to supplement and ideally replace solvothermal chemistry with less wasteful activation approaches. Mechanically activated organic chemistry (5)—in which force, rather than heat and solvent or hydrostatic pressure, drives the making and breaking of covalent bonds-can help to ameliorate the waste and energy challenges of organic synthesis because the reactions are run neat or with minimal solvent (6), and energy can be provided more efficiently through mechanical rather than thermal means (7). Even when solvents are added to mechanochemical reactions, in a process called liquid-assisted grinding, they are added in comparatively small amounts (8). Another benefit is that mechanochemically activated conditions often produce stereoisomers and regioisomers that are not favored, or cannot be produced at all, under solvothermal conditions (9), although why such mechanically favored products arise is often not well understood.

¹The Advanced Science Research Center, Graduate Center of the City University of New York, New York, NY 10031, USA. ²Department of Chemistry, Hunter College, New York, NY 10065, USA. ³Ph.D. Program in Chemistry, Graduate Center of the City University of New York, New York, NY 10016, USA. ⁴Department of Mechanical Engineering and Applied Mechanics, University of Pennsylvania, Philadelphia, PA 19104, USA. ⁵Department of Mechanical Engineering, University of California, Merced, CA 95343, USA. *Corresponding author. Email: abraunschweig®gc.cuny.edu

Despite its many potential advantages, organic mechanochemistry has not been widely adopted in chemical synthesis and manufacturing. This can be attributed in part to substantial remaining gaps in the understanding of reaction kinetics under mechanochemical activation. Until physical models are developed that reliably account for experimental observations, the products of mechanochemical reactions cannot be predicted, and the reactions cannot be easily translated to large scales. Mechanochemical reactions are typically carried out in ball mill (10) or planetary mill reactors (11) or in twin-screw extruders (12), for which it is difficult to determine even the most basic reaction parameters, such as the magnitude of the applied force (F), the reaction time under force (t), or conversion at different time points. Polymer mechanochemistry (13-15) entails the use of mechanical energy to activate mechanophores (16-18) embedded within long polymer chains: Sonication (19, 20), atomic force microscopy (AFM) (21, 22), and/or laser pulses (23) apply mechanical energy that ruptures the mechanically susceptible bonds in the mechanophores. However, these methods are used to initiate bond rupture, and as a consequence, such studies do not explain bond-formation events in mills and extruders. This difficulty in acquiring quantitative experimental data on bond formation under stress complicates the development and validation of generalizable kinetic models of mechanochemical bond-forming reactions. Furthermore, because mechanochemical reactions are carried out on powders, rather than well-solvated molecules, the kinetics of grinding to expose molecular reactants adds another layer of complexity to kinetic models. For example, the rate of pericyclic [4+2] Diels-Alder cycloadditions in ball (10) and planetary (24) mills are dependent on particle size (25), shaking frequency (10), ball mass (25), and vessel loading (26) in addito the molecular-scale factors that are known to affect rates, such as reactant structure and temperature (T) (27).

Given all these macroscopic factors, it has been challenging to explain how mechanical energy acts on the reaction potential energy surface. One such explanation is the "hotspot" model (28), which postulates that localized heating occurs when milling balls collide with surfaces and with each other, causing the release of kinetic energy. Rate increases in mechanochemical reactions are thus posited to arise because of conventional thermal activation at the collision sites. Although some local heating is observed upon milling, these temperature increases are small and are not commensurate with observed reaction rate increases (29). The other dominant kinetic theory of mechanochemistry argues that grinding increases the surface area of powders, increasing the collision probability of reactants, which explains the dependence of rates on powder size (25). Ultimately, current kinetic models of organic mechanochemistry-the molecular-scale hotspot theory and the macroscopic model that considers increases in area during grinding-are incomplete because they fail to account for all experimental observations. In particular, they fail to account for the formation of different isomers under mechanochemical activation versus strictly solvothermal activation, which indicates that F can move reactants along a different reaction trajectory than that from heat. As such, any accurate molecular-scale kinetic model of mechanochemical reactions must consider how F distinctly alters reaction trajectories and explain quantitatively how F affects reaction barriers and, in turn, reaction rates. With the physical understanding inherent to an accurate molecular-scale model of mechanical reactivity, the reactions that are susceptible to mechanical activation could be anticipated and their rates and products predicted accurately, leading to the wider adoption of sustainable mechanochemical methods in organic synthesis and chemical manufacturing.

We experimentally and computationally investigated the reaction kinetics of mechanically activated [4+2] Diels-Alder cycloaddition reactions between dienophiles and surfaceconfined diene monolayers to measure how force affects reaction rates. Pericyclic reactions were chosen because they proceed in concerted fashion without intermediates (30). which minimizes challenges in analyzing their kinetics. The reactions were carried out on monolayers so that the complexities associated with grinding powders during milling and reactant availability were not factors in the kinetic analysis, and the effects of F on the free energy of activation (ΔG^{\ddagger}) and reaction trajectories would be isolated. The experiment

(Fig. 1) used elastomeric arrays (figs. S7 and S23) that contained 900 pyramidal tips with heights of 21.9 µm and base edge lengths of 31 µm (31, 32) to bring fluorescently labeled dienophiles into contact with monolayers of the tethered diene, anthracene, that was immobilized covalently onto the surface of a silica (SiO_2) wafer (33, 34). The tip arrays were mounted onto piezoactuators so that they could be pushed into the monolayer with precise control over F and t (32, 35, 36), resulting in a nanoreactor where the anthracene and dienophile react under mechanical activation. The tips themselves were coated with an ink mixture that consisted of a large excess of the fluorescent dienophiles embedded within a polymer matrix that solubilized the dienophiles and ensured that they were accessible to react with the immobilized anthracene (37). We used fluorescence microscopy to track the

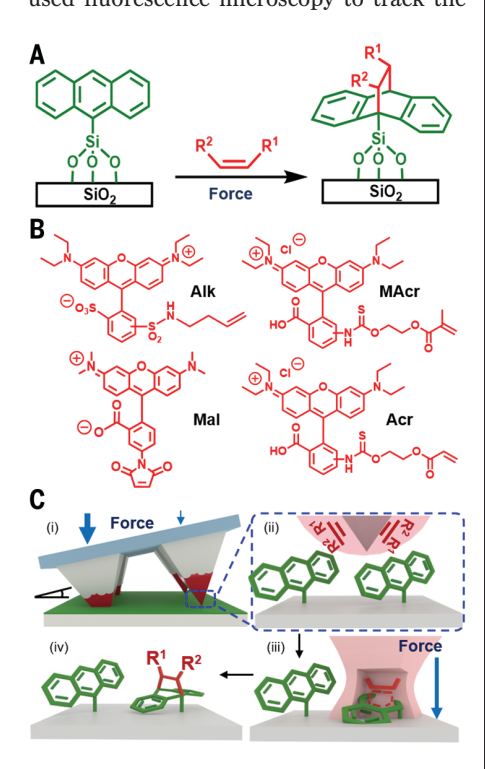


Fig. 1. Force-activated Diels-Alder reactions on anthracene monolayers. (A) Diels-Alder cycloaddition reaction between anthracenes immobilized onto SiO₂ surfaces and dienophiles under applied force. (B) Structures of dienophiles Alk, Mal, MAcr, and Acr. (C) (i) Elastomeric tip arrays transfer an ink mixture (red coating), consisting of a dienophile and PEG, onto an anthracene-modified surface. The tip arrays are tilted so that different forces are applied by the tips at different locations across the surface. Thick arrows indicate areas of the tip array that exert high force, and thin arrows indicate areas that exert low force. (ii) Upon contact with the surface, the tips form nanoreactors, (iii) where forces are applied that accelerate the Diels-Alder cycloaddition reactions. (iv) After washing the surface, only covalently bound molecules remain on the surface.

Diels-Alder adduct formation as a function of F and t. We studied the reaction rates of the anthracene monolayer with four different dienophiles-an alkene (Alk), a maleimide (Mal), a methacrylate (MAcr), and an acrylate (Acr)-because they differ in the electron demand (38) and the steric environment (39) around the reactive alkene, factors that affect the reaction rates of Diels-Alder reactions (27, 30) under strictly solvothermal conditions. which allowed us to examine how mechanochemical reactivity trends differ from strictly solvothermal trends. We determined the pressure (p) of the reaction using a scale below the tips and finite element analysis modeling (FEM). The fluorescence data were fit to a first-order kinetic model to determine activation parameters, including the activation energy (E_a) , which is the energy difference between the transition state and the initial state in the absence of stress; ΔG^{\ddagger} ; and the activation volume (ΔV^{\dagger}), which is a measure of the sensitivity of a reaction to mechanical activation (40, 41). These data reveal that rate constant (k) increases of a factor of >10× occur at only a few atmospheres of p, and the sensitivity of this experimental approach is such that the effects of subtle differences in dienophile structure on rates could be determined, revealing that mechanochemical reactivity trends are distinct from solvothermal trends. Molecular dynamics (MD) and density functional theory (DFT) modeling of the surface and reaction revealed how molecular distortions account for changes in ΔG^{\ddagger} , providing a generalizable model for mechanochemical reactivity that suggests that the scope of mechanically susceptible reactions may be substantially broader than previously anticipated.

Experimental setup

For the printing experiment, we modified an approach we have developed for studying mechanochemical surface reactions quantitatively (31, 32), in which the reactions occur under a ~1-cm² elastomeric polymer tip array (42, 43). The inked 900-tip arrays were mounted onto the z-piezoactuator of an atomic force microscope equipped with a specialized mount for the tip arrays and an x,y-tilting stage. Upon moving the arrays in and out of contact with the surface, each tip in the array prints a twoby-five array of 10 features, in which each feature in a two-by-five array is printed with a different tip-surface contact time t that varies from 1 to 600 s. The substrate is intentionally tilted with respect to the tip-array so that the F applied by individual tips varies systematically across one axis of the surface (36). In this experiment, the effect of 30 different values of F, ranging from 1.91 to 89.4 μ N (table S1), and 10 different values of t on reaction conversion could all be assessed from a single printed surface. In addition, each two-by-five pattern generated at a given F is repeated 30 times by the tip arrays, resulting in denser data sets that enable higher-fidelity fitting. After printing, the surface was sonicated in ethyl alcohol (EtOH) for 5 min to remove any physisorbed dienophile and polyethylene glycol (PEG) from the substrate, and F, k, $E_{\rm a}$, ΔV^{\dagger} , and ΔG^{\ddagger} values for the reaction between a fluorescent diene and surface-bound anthracene could be determined from the normalized fluorescence intensity I (fluorescence of feature/fluorescence of background) from images taken from a single printed surface.

Characterization of patterned surfaces

We relied on several complementary analytical techniques to confirm the formation of the anthracene monolayer and, subsequently, the formation of the Diels-Alder adduct. Fluorescence intensity data derived from fluorescence microscopy images (Fig. 2A) confirmed that the immobilization of the fluorophores occurs only where the tips contact the surface, and that I is dependent on both F and t (Fig. 2B). Time-of-flight secondary ion mass spectrometry (ToF-SIMS) data (Fig. 2C) show that fluorescent features of the two-by-three patterns are chemically distinct from unprinted areas, with the spectra of the former containing features consistent with the presence of the dienophile, whereas the latter are consistent with an unreacted anthracene monolayer. X-ray photoelectron spectroscopy (fig. S3), contact angle measurements (fig. S6), and AFM imaging (fig. S13) were carried out, and all data are consistent with the proposed modified surfaces. Control experiments (fig. S12), including patterning of the fluorophores onto a bare SiO₂ surface or the patterning of dyes that lack the reactive alkene onto anthracene surfaces, failed to produce fluorescence patterns, further confirming that the fluorescent patterns are the result of the covalent bond formation that occurs during the Diels-Alder cycloaddition. Although no single surface technique is capable of directly confirming the formation of new covalent bonds in monolayers, the totality of the data makes any explanation of the fluorescent patterns for a reason other than covalent bond formation through a [4+2] Diels-Alder reaction unlikely.

Determination of activation parameters

To analyze the fluorescence data and extract kinetic parameters, we assumed that the Diels-Alder reaction in this system follows a first-order kinetic rate law (eq. S10) and that fluorescence images can be used to quantify conversion as a function of F and t. We adopted the pseudo-first order assumption because at the interface, the dienophile concentration is substantially greater than the anthracene concentration. We have previously applied this same model to the kinetic data of other

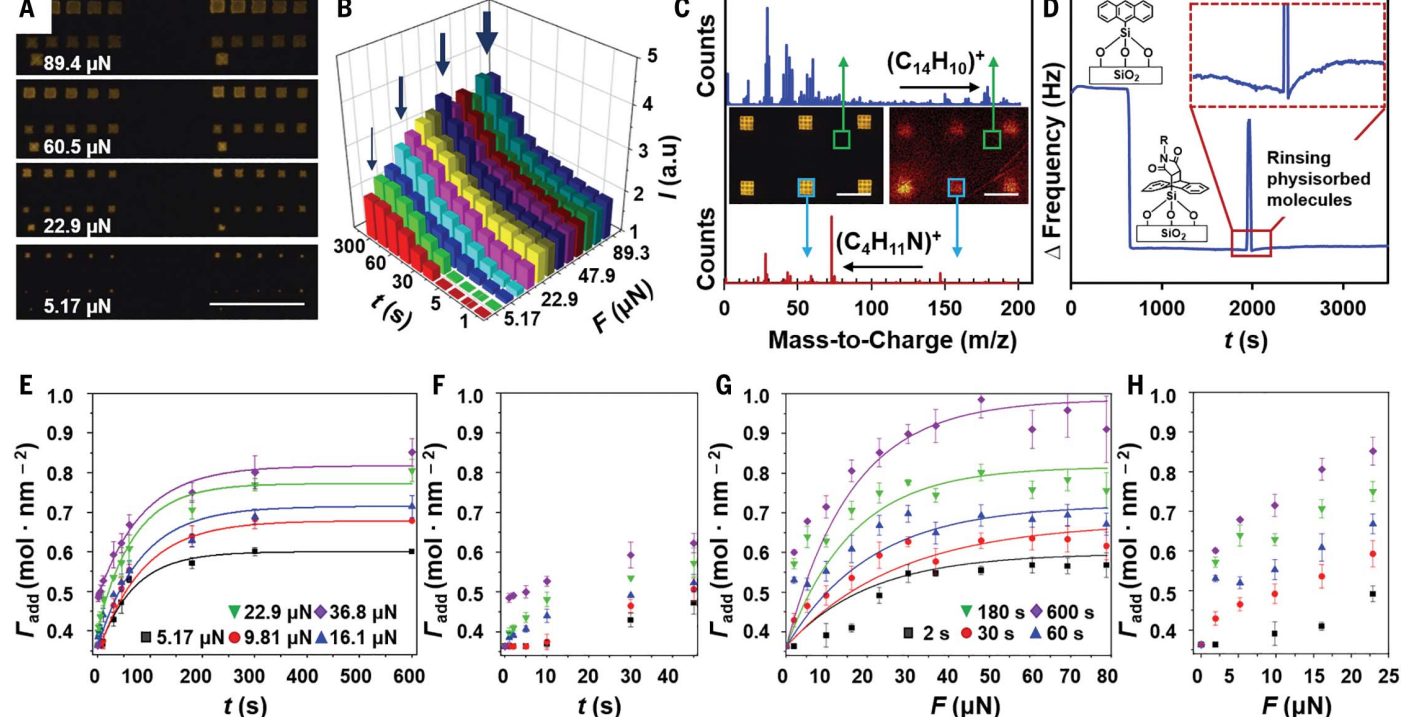


Fig. 2. Experimental data for Diels-Alder reactions on anthracene monolayers with varying force and times. (A) Fluorescence image (λ_{ex} = 530 to 550 nm and λ_{em} = 575 to 750 nm, where λ_{ex} is the excitation wavelength and λ_{em} is the emission wavelength), observed after washing and sonication, of surfaces after patterning with fluorescently labeled dienophile Alk onto the anthracenemodified SiO₂ surface. The imaged areas vary from high (top) to low (bottom) F applied to the substrate during the cycloaddition reaction by the tilted tip arrays. Scale bar, 90 µm. (B) Normalized fluorescence intensity (1 is fluorescence of feature/fluorescence of background) of the printed features of Alk as a function of F and t. Arrows above the bars indicate the data taken from the fluorescent images in (A); the wide arrows indicate high F, and narrow arrows indicate low F. (C) Time-of-flight secondary-ion mass spectrometry (ToF-SIMS) map (positive ion mode) of a surface patterned with Alk after sonication and washing. (Middle left) Fluorescent image. (Middle right) Corresponding ToF-SIMS map.

Scale bar, 100 µm. Mass spectrometer data were taken from unreacted (top) and reacted (bottom) areas of the surface. The peak at mass/charge ratio (m/z) = 178.08 is identified as a $C_{14}H_{10}^{+}$ fragment corresponding to anthracene, and the peak at m/z = 73.01 is identified as a $C_4H_{11}N^+$ fragment corresponding to the secondary dialkyl amine of the rhodamine dye. (D) OCM measurement tracking the formation of the Diels-Alder adduct from the reaction of Mal with anthracene-functionalized QCM crystal in PhMe solution. The abrupt drop in the frequency corresponds to the introduction of new solutions into the OCM. The spike in the frequency and inset correspond to the introduction of a solution of EtOH to wash physisorbed molecules from the surface. (E and F) Plots of surface density of the adduct (Γ_{add}) versus t for the reaction of **Alk** with the anthracene surface. (${\bf G}$ and ${\bf H}$) Plots of $\Gamma_{\rm add}$ versus F for the reaction of ${\bf Alk}$ with the anthracene surface. Error bars are 1 SD from the mean of three independent measurements. Fits were weighted to the error bars.

pericyclic reactions on monolayers under applied F and found good agreement between the model and the experimental data (32). To determine the rate constant k, it was necessary to track conversion of anthracenes on the surface to adduct by measuring the grafting density of the anthracene (Γ_{anth}) and of the adduct (Γ_{add}) in the fluorescent features. A quartz crystal microbalance (QCM) measurement on a SiO2 crystal that was subjected to the anthracene monolayer formation protocols provided $\Gamma_{\text{anth max}}$, the concentration of anthracene in the unreacted monolayer, of $1.12 \pm 0.33 \text{ mol} \cdot \text{nm}^{-2}$ (fig. S18), which is in good agreement with the value obtained from MD simulations of $\Gamma_{anth,max} = 1.20 \pm 0.08 \text{ mol} \cdot \text{nm}^{-2}$ (figs. S36 and S37). The maximum grafting density of the adduct (\Gamma_{add.max}) was determined by monitoring the reaction between an anthracenemodified QCM crystal and a solution of Mal within the fluid cell of the QCM (Fig. 2D). This reaction was selected because it occurs

rapidly, even in the absence of F, so that the reaction would proceed to completion in the QCM. The QCM data were consistent with the formation of the adduct with $\Gamma_{add,max}$ = $0.94 \pm 0.14 \text{ mol·nm}^{-2}$, suggesting that only 75 to 84% of the anthracene can react with Mal, at which point the surface is saturated with adduct. For the ensuing calculations, we assumed that the adducts that formed with the different dienophiles had similar volumes and, in turn, similar $\Gamma_{add,max}$. An accurate measure of F at each feature was needed to understand the relationship between reaction rate and F. We determined F using a balance below the printed surface and measuring the recorded weight and feature edge length (fig. S22 and table S1) (35), and these calculations determined that the F across the substrate ranged from 1.91 to 89.4 µN. We conducted FEM of individual pyramidal tips to validate the force measurements, and the relationship between feature length and z-displacement matched the experiments and was nearly independent of the assumed elastic constants for polydimethylsiloxane (PDMS). Furthermore, the values of the simulated F as a function of z-piezo extension could be readily fit to the experimental data by using values of the PDMS elastic constants well within typical measured values (figs. S23 and S24). Last, we considered whether surface roughness could create localized asperities of high force and found that average surface roughness (0.41 nm) (fig. S25) was too low to cause any noteworthy effect.

With these data in hand, the surface density of the adduct (Γ_{tF}) could be determined from the fluorescence intensity of the features printed at different F and t from $I_{t,F}$ using Eq. 1

$$\Gamma_{t,F} = \left[1 - \left(\frac{I_{\rm max} - I_{t,F}}{I_{\rm max}}\right)\right] \cdot \Gamma_{\rm add,max} \eqno(1)$$

where I_{max} is the fluorescence intensity of a feature that has reached saturation with the adduct. This equation assumes $\Gamma_{t,F}$ and $I_{t,F}$

are linearly related, an assumption that can be used in organic monolayers when the fluorophores do not couple (44). The relationship between $\Gamma_{t,F}$, F, and t for each feature was plotted for all anthracene-dienophile pairs (Fig. 2, E to H, and figs. S27 to S30). In all cases, we observed that $\Gamma_{t,F}$ increased with increasing t and F. Mal is the only dienophile that formed adduct in the absence of F, and the rate quickly reached a maximum upon the application of minimal F. This is consistent with known trends for Diels-Alder reactions with normal electron demand, in which the presence of electron withdrawing groups on the dienophile lowers the E_a (27, 30). The plots of Γ_{tF} versus t (Fig. 2, E and F) and Γ_{tF} versus F (Fig. 2, G and H) fit well to a first-order rate model, further validating the pseudofirst order assumption. All fits of kinetic data were weighted to the error bars, and χ^2 analysis showed that the fits were statistically significant at a 95% level of confidence.

A mathematical framework was needed to derive the activation parameters k, E_a , ΔV^{\dagger} , and ΔG^{\ddagger} from the experimental data. We adapted the model, developed from examining chemical reactions under hydrostatic pressure (45, 46) and based on the work of Evans and Polanyi (47) and Eyring (48), that considers how p affects k. Under hydrostatic pressure, cycloaddition reactions have finite and negative ΔV^{\dagger} , meaning that p will increase k according to Eq. 2

$$\ln(k) = \ln(A) - \frac{E_{\rm a}}{k_{\rm B}T} - \frac{p\Delta V^{\ddagger}}{k_{\rm B}T} \qquad (2)$$

where A is the preexponential factor, T is the temperature, and $k_{\rm B}$ is Boltzmann's constant. This model, which considers the effects of thermal and mechanical activation on the rate, has $\Delta G^{\ddagger} = E_{\rm a} + p\Delta V^{\ddagger}$. We follow the convention, used broadly in the study of the effects of p on chemical kinetics, in which a negative ΔV^{\ddagger} acts to reduce ΔG^{\ddagger} . To apply this model, the mean p in the nanoreactor contacts was determined as a function of F by dividing by the feature area. Our use of mean pressure is consistent with current pub-

lished work on probe-based mechanochemistry (32, 49, 50). There was a spatial distribution of that pressure, as seen in our finite element simulations (fig. S23D), but this does not alter the observed trends nor our primary conclusion that nonhydrostatic compression increases reaction rates as a result of molecular distortion, lowering the reaction energy.

With these experimental data, we determined all the activation parameters of interest for each dienophile-anthracene pair. Isothermal first-order Arrhenius plots of $\ln\Gamma_{\rm anth}$ versus twere fitted, and k at each pressure was determined from the best-fit linear correlation (Fig. 3A and fig. S31) that was weighted to the error bars; errors are reported as the standard error of the fit. For **Alk**, k increased from 3.8 \pm $0.25 \times 10^{-3} \text{ s}^{-1}$ at p = 0.16 MPa to $1.55 \pm 0.19 \times$ 10^{-2} s⁻¹ at p = 0.32 MPa, and this trend of increasing k with increasing p is consistent throughout all the data. The greatest change in k was observed for **MAcr** (from 4.07 \pm 0.58×10^{-3} to $1.77 \pm 0.77 \times 10^{-1}$ s⁻¹) and the smallest for **Mal** (from 4.0 \pm 0.050 \times 10^{-2} to $1.57 \pm 0.77 \times 10^{-1} \text{ s}^{-1}$). The $E_{\rm a}$ and ΔV^{\sharp} were determined from the extrapolated y-intercept and slope, respectively, of the linear fit of the plot of $\ln k$ versus p (Fig. 3B). The E_a follow the trend MAcr > Acr > Alk > Mal. The magnitudes of E_a in the anthracene monolayers, 84.5 to 96.4 kJ·mol⁻¹, are similar in magnitude to values for Diels-Alder reactions with anthracene reported in the literature of 63.6 to 83.7 kJ·mol⁻¹ (51, 52), and these small differences in magnitude in the E_a between reactions in solution and monolavers can be attributed to differences in molecular structures, reaction geometry, lack of solvent, and the influence of the SiO₂ surface. All ΔV^{\ddagger} are negative, and the differences in ΔV^{\ddagger} between the dienophileanthracene pairs reflect the relative susceptibilities of their rates to mechanically induced pressure. The ΔV^{\ddagger} range from -60.7 × $10^{3} \text{ cm}^{3} \cdot \text{mol}^{-1} \text{ for } \mathbf{MAcr} \text{ to } -21.8 \times 10^{3} \text{ cm}^{3} \cdot \text{mol}^{-1}$ for Mal and follow the identical trend of **MAcr** > **Acr** > **Alk** > **Mal**, meaning that the reactions with larger E_a are more sensitive to mechanochemical activation. Also, these ΔV^{\dagger}

values are substantially greater than the ΔV^{\dagger} of -20 to -45 cm³·mol⁻¹ for Diels-Alder reactions observed (46) under hydrostatic p in solution, where interfaces do not have a role in the reaction. Last, we calculated the change in free energy of activation $\Delta \Delta G^{\ddagger} = p \Delta V^{\ddagger}$ at every p for each dienophile-anthracene pair (Fig. 3C) and found that $\Delta \Delta G^{\dagger}$ range from -3.53 to -19.46 kJ·mol⁻¹, with an average value of -8.21 kJ·mol⁻¹, which would cause a ~14-fold rate increase in rate. The relative sensitivity to p shown in Fig. 3B was validated by adding the rhodamine-labeled Mal (Fig. 3B, red) and a MAcr that was labeled with fluorescein (Fig. 3B, green) to the same tip array (fig. S33) and then printing them simultaneously (fig. S34). which led to the fluorescence intensity of the red dye remaining constant as force was increased, whereas the intensity of the green dye increased with increasing force (fig. S35).

Modeling mechanical distortion

We used DFT calculations to generate a theoretical model for the energetics of the reactants and the transition states (TSs) and to understand mechanistically how F acts on the system to lower the reaction energy (ΔE). Although experiments determined ΔG^{\ddagger} , our calculations and the ensuing theoretical treatment involve ΔE , which is the reaction energy that does not take into account vibrational and entropic effects that are not included in the DFT calculations. Anthracene was simulated as attached to a Si₄O₉H₃ cluster to mimic the effect of the surface. DFT calculations predicted the E_a , which is the activation energy for the strictly solvothermal reactions, as defined by Eq. 2, for the Diels-Alder reaction to be between 77.1 (Mal) and 90.0 (Alk) kJ·mol⁻¹ (Fig. 4A and fig. S44). These values are within range of the experimental values. The overestimation of the E_a of **Alk** is likely caused by limiting the reaction system to the anthracene, SiO2 cluster, and dienophile. In doing so, we neglected the destabilizing effects caused by the interactions between the surrounding SiO2 surface and the rhodamine fluorophore. This omission led to interactions

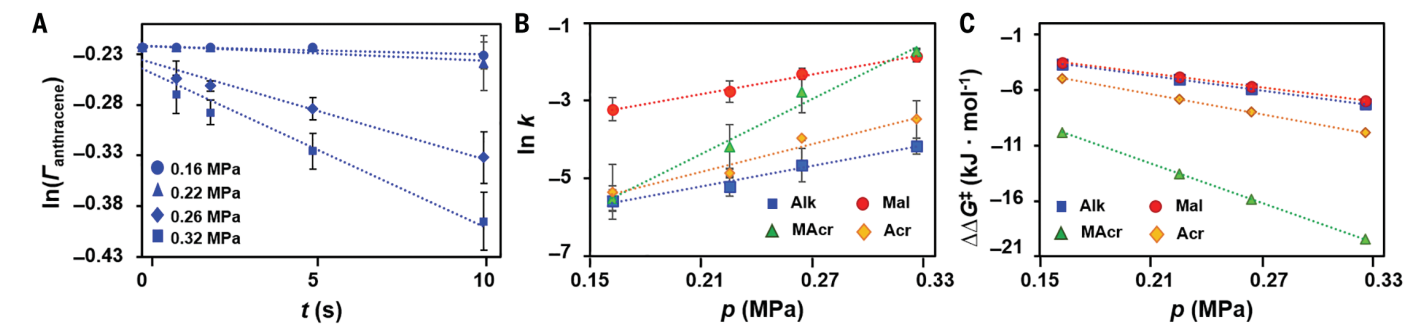


Fig. 3. Activation parameters for the Diels-Alder reactions on anthracene monolayers. (A) Isothermal Arrhenius plots of $In(\Gamma_{anthracene})$ versus t at different F for the reaction between **Alk** and the anthracene monolayers. Fits are based on eq. S12. The slope of these lines provide k. (B) Plot of Ink versus p for all four dienophiles, the slope of which provides ΔV^{\ddagger} , whereas y-intercept provides E_a . Fits were weighted to the error bars, and coefficients of determination (R^2) are 0.97 to 0.99. (C) $\Delta\Delta G^{\ddagger}$ as a function of p.

in the calculations that stabilized the Alkanthracene reactant complex, resulting in a higher reaction barrier than was measured experimentally. MD simulations showed that the anthracene responds to tip-induced compression by bending toward the surface, that the fraction of molecules with distorted CCH angles increases with increasing pressure (fig. S42), and that compression causes deformation of the molecules themselves (figs. S40 to S42). To model the effect of the mechanical distortion caused by uniaxial stress acting on the reactant from the top, we used DFT to distort the anthracene along three angles-OSiC, SiCC, or CCH (Fig. 4A)—and the geometry of the reactant and TS were fully relaxed, while keeping those angles fixed. In this model, we envision that F increases the energy of the reactants by distorting the anthracene in a way that increases its reactivity. The acceleration of the reaction can be then achieved when the distortion energy of the reactants $(\Delta E_{\rm d}^{\rm R})$ is larger than the distortion energy of the TS $(\Delta E_{\rm d}^{\rm TS})$ (53). The change in the reaction energy $(\Delta \Delta E)$ that oc-

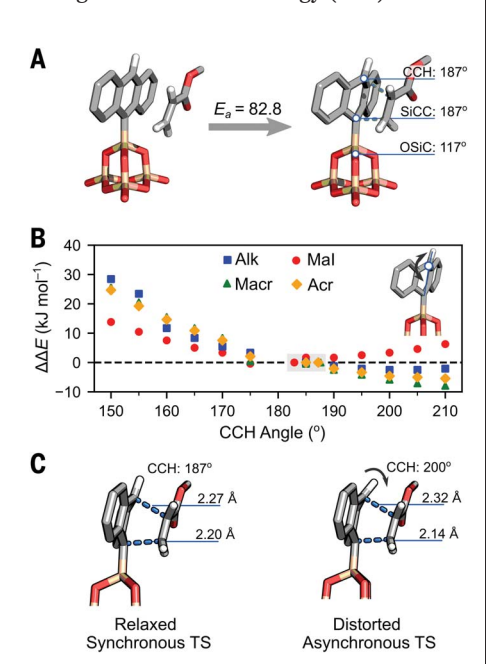


Fig. 4. Mechanical distortion under uniaxial stress. (**A**) The activation energy E_a and the geometry of the relaxed transition state involving **Acr**. Blue lines indicate OSiC, SiCC, and CCH angles, distortion of which by the applied F is explored in (B) and (C). All calculations have been performed at M06-2X/6-311+G(d,p) level of theory (31, 32, 57, 58). (**B**) The relative change ($\Delta\Delta E$) to the reaction energy (ΔE) as a function of the CCH angle. The gray box indicates the fully relaxed TS geometry. The bending of the CCH angle leads to the decrease of the ΔE for **MAcr**, **Acr**, and **Alk**. (**C**) The effect of distorting the CCH coordinate on the geometry of the TS. Pushing the H atom toward the dienophile creates an asynchronous TS, which lowers the reaction energy.

curs during the distortion of the anthracene reactant and TS are shown in Fig. 4B and fig. S45. We observed that distorting the anthracene along OSiC and SiCC angles increases ΔE . However, bending the top H (CCH) toward the dienophile, from the relaxed geometry of between 180° and 190° to 200°, decreases the ΔE of **Alk**, **Acr**, and **MAcr** by 2.6, 4.4, and 5.6 kJ·mol⁻¹, respectively, which is consistent with the experimentally determined $\Delta \Delta G^{\dagger}$ and follows the identical trend MAcr > Acr > Alk > Mal. Only in the case of Mal did bending of the CCH angle increase the ΔE , most likely because of repulsive electrostatic interactions between the bulky dienophile and the SiO₂ cluster, although this is still consistent with the smallest $\Delta \Delta G^{\ddagger}$ observed experimentally for Mal. Subsequently, we explored the effect of bending of other angles or bending multiple angles simultaneously (fig. S46 and table S14), and these calculations did not result in substantially different values of ΔE . This particular bending motion is productive because it increases asynchronicity-the difference in length (Δr_{C-C}) between newly formed C-C bonds-of the TS (Fig. 4C). This deformation from the relaxed, nearly synchronous TS of the **Acr** $(\Delta r_{C-C}^{Acr} = 0.07 \text{ Å})$ to the distorted, asynchronous TS $(\Delta r_{C-C}^{Acr} = 0.18 \text{ Å})$ reduces the destabilizing activation strain and unfavorable Pauli repulsion between the reactants. which results in a lower ΔE (53, 54). Furthermore, the predicted degree of the asynchronicity of the distorted TSs (table S13) is consistent with the increasing acceleration of the reaction. **MAcr** > **Acr** > **Alk** > **Mal**.

Mechanical force, which acts as uniaxial compression, modifies the potential energy surface of the Diels-Alder reaction differently than does hydrostatic pressure. Under strictly solvothermal conditions (Fig. 5A), ΔE is equal to the strictly solvothermal activation energy $E_{\rm a}$. Hydrostatic pressure (Fig. 5B) acts along the reaction coordinate by reducing the energy of the transition state ($\Delta E_{\rm H}^{\rm TS}$), and $\Delta \Delta E$ = $\Delta E_{\rm H}^{\rm TS} = p \Delta V^{\ddagger}$. ΔV^{\ddagger} of Diels-Alder reactions under hydrostatic pressure are modest (-20 to -45 cm³·mol⁻¹) (46) because hydrostatic pressure squeezes equally along three axes and does not cause molecular distortion. As such, a p of ~150 MPa is needed for a $\Delta\Delta E$ of -4.4 kJ·mol⁻¹, which is an arbitrarily chosen value of $\Delta\Delta E$ that is in the range of those $\Delta\Delta G^{\dagger}$ measured here experimentally. Uniaxial compression (Fig. 5C) distorts the reactants, raising their energy by $\Delta E_{\rm d}^{\rm R}$, and also distorts the transition state to raise its energy by $\Delta E_{\rm d}^{\rm TS}$. So, under mechanochemical conditions, in which uniaxial compression can cause distortions to occur, $\Delta\Delta E = \Delta E_{\rm d}^{\rm TS} - \Delta E_{\rm d}^{\rm R} = p\Delta V^{\ddagger}$. Because the magnitudes for the ΔV^{\ddagger} we observed for mechanically distorted Diels-Alder reactions are large (> 10^4 cm 3 ·mol $^{-1}$), the same $\Delta\Delta E$ of $-4.4 \text{ kJ} \cdot \text{mol}^{-1}$ can be achieved at p < 1 MPa.

We also found that similarities exist (fig. S47) in how force modifies the potential energy surfaces of mechanochemical bond formation (pushing, which causes uniaxial stress) and mechanochemical bond rupture reactions (pulling, which involves uniaxial stress in the opposite direction). In 2007, Hickenboth et al. studied bond rupture in another pericyclic reaction, the ring opening of a benzocyclobutene mechanophore, while using sonication to drive the ring-opening reaction (20). Since then, other pericyclic reactions, including the retro Diels-Alder reaction driven by pulling, have also been examined (17, 22). The Diels-Alder reaction (bond forming) and benzocyclobutene ring-opening-retro Diels-Alder reactions (bond rupture) are all pericyclic reactions, meaning that their regioselectivities and stereoselectivities are governed by the Woodward-Hoffmann rules. The studies by Hickenboth et al. first revealed that a distorted state also precedes the TS and bond rupture in ring opening, and the result of this distorted state is a decrease in ΔE , where the relationship $\Delta \Delta E$ = $\Delta E_{\rm d}^{\rm TS} - \Delta E_{\rm d}^{\rm R}$, the same relationship that we observed for mechanochemical bond formation, also applies. Thus, the key to understanding regioselectivity and stereoselectivity in mechanochemical pericyclic reactions—and bringing mechanochemically driven pericyclic reactions within the Woodward-Hoffmann manifoldnecessitates understanding the distortion that uniaxial mechanical stress induces in the reactants and the TSs. There is, however, an important difference between how pushing and pulling modify the reaction potential energy surface: a Diels-Alder reaction driven by compression will follow a distinct trajectory along the potential energy surface than the retro Diels-Alder reaction of its products. As such, the geometries and energies of the TSs and the distorted states of the Diels-Alder reaction and the retro Diels-Alder reaction will be very different.

We have used elastomeric tip arrays to control precisely the t and F applied between dienes and dienophiles on a surface to determine $k, E_a, \Delta V^{\dagger}, \Delta G^{\dagger}$, and $\Delta \Delta G^{\dagger}$ for the Diels-Alder reaction between immobilized anthracene and four dienophiles that differ in steric and electronic demand. We found that ΔV^{\dagger} is ~1000-fold greater on surfaces under uniaxial compression than under hydrostatic pressure, indicating that the reactions follow different trajectories. The value of tip-based approaches for measuring the kinetic parameters of mechanochemical bond-breaking reactions is well known, and in this work we show that the techniques are equally valuable for studying bond-forming mechanochemical reactions. These results have important implications for the study, understanding, and wider application and adoption of mechanochemistry. These results also explain that the large ΔV^{\ddagger} for mechanochemical reactions occur as a result

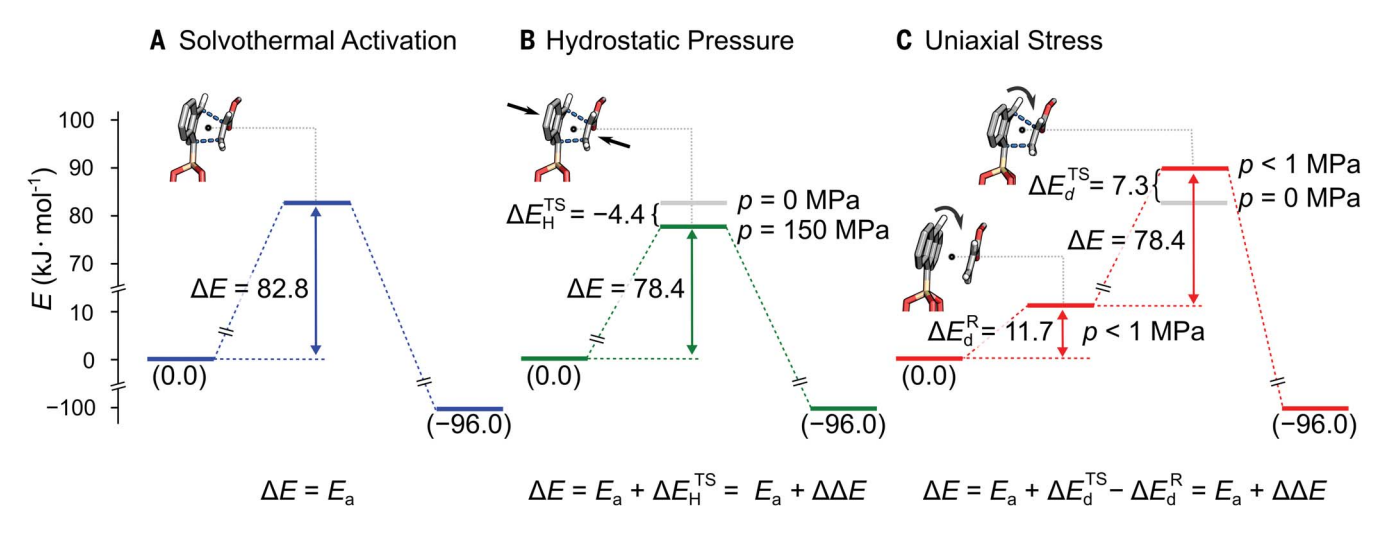


Fig. 5. Comparison of reaction trajectories under strictly solvothermal activation, hydrostatic pressure, and uniaxial stress. (A) Reaction potential energy diagram of the Diels-Alder reaction under strictly solvothermal activation. (B) Reaction potential energy diagram of the Diels-Alder reaction under hydrostatic pressure. The arrows indicate the hydrostatic forces that accelerate the reaction. ΔE_{H}^{TS} was calculated by using ΔV^{\ddagger} of $-30 \text{ cm}^{3} \cdot \text{mol}^{-1}$ to predict the change in the ΔE in the hydrostatic mechanism at a p of 150 MPa.

(C) Reaction potential energy diagram of the Diels-Alder reaction under uniaxial

mechanochemical activation. The arrows indicate the deformation of the CCH angle on the diene from the solvothermal TS value of 187° to the arbitrarily chosen distorted TS value of 200° and associated reactant deformation energy (ΔE_d^R) and TS deformation energy (ΔE_d^{TS}) . All calculations have been performed at M06-2X/6-311+G(d,p) level of theory. The equations for calculating the reaction energy (ΔE) in each of the three reaction conditions—solvothermal activation, hydrostatic pressure, and mechanical distortion—are provided below the potential energy diagrams.

of the proximity to surfaces and uniaxial stress that cause molecular distortion. This distortion lowers the reaction energy and drives the reaction through a distinct reaction trajectory, which explains why different isomers are often obtained under F than in solvent (9, 55). This phenomenon-the distortion of molecules near surfaces that occurs under F to lower ΔG^{\ddagger} will be relatively independent of molecular structure and suggests that mechanochemical reactivity is more widespread than previously anticipated. As a consequence, these results should encourage the adoption of mechanochemical methods for sustainable chemical synthesis and for accelerating reactions that are otherwise impractically slow.

REFERENCES AND NOTES

- 1. S. G. Koenig et al., ACS Sustain. Chem.& Eng. 7, 16937-16951 (2019).
- 2. R. K. Henderson et al., Green Chem. 13, 854-862 (2011).
- D. R. Joshi, N. Adhikari, J. Pharm. Res. Int. 28, 1-18 (2019).
- US Energy Information Administration, "2018 Manufacturing Energy Consumption Survey" (US Energy Information Administration, 2021).
- G.-W. Wang, Chem. Soc. Rev. 42, 7668-7700 (2013).
- H. P. DeGroot, T. P. Hanusa, Organometallics 40, 3516-3525 (2021).
- J.-L. Do, T. Friščić, ACS Cent. Sci. 3, 13-19 (2017).
- T. Friščić, C. Mottillo, H. M. Titi, Angew. Chem. Int. Ed. 59, 1018-1029 (2020).
- J. G. Hernández, C. Bolm, J. Org. Chem. 82, 4007-4019 (2017).
- 10. J. M. Andersen, J. Mack, Chem. Sci. 8, 5447-5453 (2017).
- 11. F. J. Gotor, M. Achimovicova, C. Real, P. Balaz, Powder Technol. 233, 1-7 (2013).
- 12. D. Crawford et al., Chem. Sci. 6, 1645-1649 (2015).
- 13. P. A. May, J. S. Moore, Chem. Soc. Rev. 42, 7497-7506 (2013).
- 14. J. Li, C. Nagamani, J. S. Moore, Acc. Chem. Res. 48, 2181-2190 (2015).
- 15. A. L. Black, J. M. Lenhardt, S. L. Craig, J. Mater. Chem. 21, 1655-1663 (2011).
- 16. J. Li et al., J. Am. Chem. Soc. 136, 15925-15928 (2014)

- 17. J. Wang et al., Nat. Chem. 7, 323-327 (2015).
- 18. G. R. Gossweiler et al., ACS Macro Lett. 3, 216-219 (2014).
- 19. K. L. Berkowski, S. L. Potisek, C. R. Hickenboth, J. S. Moore, Macromolecules 38, 8975-8978 (2005).
- 20. C. R. Hickenboth et al., Nature 446, 423-427 (2007).
- 21. M. Horst et al., J. Am. Chem. Soc. 143, 12328-12334 (2021).
- 22. A. R. Sulkanen et al., J. Am. Chem. Soc. 141, 4080-4085 (2019). 23. J. Sung, M. J. Robb, S. R. White, J. S. Moore, N. R. Sottos,
- J. Am. Chem. Soc. 140, 5000-5003 (2018).
- 24. J.-M. Seo, I.-Y. Jeon, J.-B. Baek, Chem. Sci. 4, 4273-4277 (2013). 25. L. Gonnet et al., ACS Sustain. Chem. & Eng. 9, 4453-4462 (2021).
- 26. K. S. McKissic, J. T. Caruso, R. G. Blair, J. Mack, Green Chem. **16**, 1628-1632 (2014).
- 27. I. Fleming, Frontier Orbitals and Organic Chemical Reactions (Wiley, 1976).
- 28. A. W. Tricker, G. Samaras, K. L. Hebisch, M. J. Realff, C. Sievers. Chem. Eng. J. 382, 122954 (2020).
- 29. H. Kulla et al., Chem. Commun. 53, 1664-1667 (2017).
- 30. I. Fleming, Pericyclic Reactions (Oxford Univ. Press, 1998).
- 31. S. Bian et al., J. Am. Chem. Soc. 135, 9240-9243 (2013).
- 32. X. Han, S. Bian, Y. Liang, K. N. Houk, A. B. Braunschweig, J. Am. Chem. Soc. 136, 10553-10556 (2014).
- 33. Y. Hong et al., J. Phys. Chem. C 123, 19715-19724 (2019).
- 34. C. Huang, H. E. Katz, J. E. West, Langmuir 23, 13223-13231 (2007)
- 35. X. Liao, A. B. Braunschweig, Z. Zheng, C. A. Mirkin, Small 6, 1082-1086 (2010).
- 36. X. Liao, A. B. Braunschweig, C. A. Mirkin, Nano Lett. 10, 1335-1340 (2010).
- 37. L. Huang et al., Small 6, 1077-1081 (2010).
- 38. J. J. Dudkowski, E. I. Becker, J. Org. Chem. 17, 201-206 (1952).
- 39. W. R. Vaughan, K. S. Andersen, J. Org. Chem. 21, 673-683 (1956). 40. B. Chen, R. Hoffmann, R. Cammi, Angew. Chem. Int. Ed. 56, 11126-11142 (2017).
- 41. A. Martini, S. H. Kim, Tribol. Lett. 69, 150 (2021).
- 42. F. Huo et al., Science 321, 1658-1660 (2008).
- 43. D. J. Eichelsdoerfer et al., Nat. Protoc. 8, 2548-2560
- 44. A. Loyter, V. Citovsky, R. Blumenthal, Methods Biochem. Anal. 33, 129-164 (1988).
- 45. C. Walling, H. J. Schugar, J. Am. Chem. Soc. 85, 607-612
- 46. T. Asano, W. J. Le Noble, Chem. Rev. 78, 407-489 (1978). 47. M. G. Evans, M. Polanvi, Trans, Faraday Soc. 31, 875-894 (1935).
- 48. H. Eyring, J. Chem. Phys. 3, 107-115 (1935).
- 49. H. Spikes, Friction 6, 1-31 (2018).
- 50. L. Fang, S. Korres, W. A. Lamberti, M. N. Webster, R. W. Carpick, Faraday Discuss. 241, 394-412 (2023).

- 51. L. J. Andrews, R. M. Keefer, J. Am. Chem. Soc. 77, 6284-6289 (1955).
- 52. K. E. Wise, R. A. Wheeler, J. Phys. Chem. A 103, 8279-8287 (1999).
- 53. F. M. Bickelhaupt, K. N. Houk, Angew. Chem. Int. Ed. 56, 10070-10086 (2017).
- 54. P. Vermeeren, T. A. Hamlin, F. M. Bickelhaupt, Phys. Chem. Chem. Phys. 23, 20095-20106 (2021).
- 55. S. Biswas et al., Faraday Discuss. 241, 266-277 (2023).
- 56. Y. Zholdassov et al., Acceleration of Diels-Alder reactions by mechanical distortion. Dryad (2023); https://doi.org/10.5061/ dryad.0cfxpnw72.
- 57. Y. Zhao, D. G. Truhlar, Theor. Chem. Acc. 119, 525-525 (2008). 58. M. Linder, T. Brinck, Phys. Chem. Chem. Phys. 15, 5108-5114 (2013).

ACKNOWLEDGMENTS

We thank P. Nautiyal for assistance with acquiring AFM images. We also thank T.-D. Li for assistance with acquiring ToF-SIMS data. Funding: A.B.B., R.W.C., and A.M. are grateful to the National Science Foundation Center for the Mechanical Control of Chemistry (CCI CHE-2023644) for generous support. A.B.B. also acknowledges award DBI-2032176 from the National Science Foundation. This work was carried out in part at the Singh Center for Nanotechnology, which is supported by the NSF National Nanotechnology Coordinated Infrastructure Program under grant NNCI-2025608. Author contributions: Y.S.Z., A.M., R.W.C., M.M., and A.B.B. conceived the research. Y.S.Z., L.Y., S.R.G., A.B., R.W.K., and D.J.V. carried out the experiments. All authors contributed to the writing of the manuscript. Competing interests: The authors declare no competing financial interests. Data and materials availability: All data are available in the supplementary materials. Tables S1 to S14 have been uploaded in more reusable tabular format to the Dryad repository (56). License information: Copyright © 2023 the authors, some rights reserved; exclusive licensee American Association for the Advancement of Science, No. claim to original US government works. https://www.science.org/ about/science-licenses-journal-article-reuse

SUPPLEMENTARY MATERIALS

science.org/doi/10.1126/science.adf5273 Materials and Methods Figs. S1 to S47 Tables S1 to S14 References (59-78)

Submitted 27 October 2022; resubmitted 14 February 2023 Accepted 13 April 2023

10.1126/science.adf5273



Acceleration of Diels-Alder reactions by mechanical distortion

Yerzhan S. Zholdassov, Li Yuan, Sergio Romero Garcia, Ryan W. Kwok, Alejandro Boscoboinik, Daniel J. Valles, Mateusz Marianski, Ashlie Martini, Robert W. Carpick, and Adam B. Braunschweig

Science, 380 (6649), .

DOI: 10.1126/science.adf5273

Editor's summary

Using ball mills to conduct chemical reactions in solid state has the potential to eliminate vast quantities of solvent waste. However, the energetics of these reactions are much harder to discern and optimize than reactions in the solution phase. Zholdassov *et al.* used a modified atomic force microscope to study in a more precise, controlled fashion how the forces squeezing molecules together in a ball mill might influence the Diels-Alder cycloaddition reaction (see the Perspective by Weiss). The authors observed much greater acceleration through mechanical distortion than hydrostatic pressure would deliver. —Jake Yeston

View the article online

https://www.science.org/doi/10.1126/science.adf5273

Permissions

https://www.science.org/help/reprints-and-permissions

Use of this article is subject to the Terms of service